Published online 7 March 2007

Nucleic Acids Research, 2007, Vol. 35, No. 7 ***e51***
doi:10.1093/nar/gkm094

Array-based profiling of reference-independent methylation status (aPRIMES) identifies frequent promoter methylation and consecutive downregulation of ZIC2 in pediatric medulloblastoma

Stefan Pfister[1,2], Christof Schlaeger[1], Frank Mendrzyk[1], Andrea Wittmann[1], Axel Benner[3], Andreas Kulozik[2], Wolfram Scheurlen[4], Bernhard Radlwimmer[1] and Peter Lichter[1,*]

[1]Department of Molecular Genetics, German Cancer Research Center, Im Neuenheimer Feld 280, 69120 Heidelberg, Germany, [2]Department of Pediatric Oncology, Hematology & Immunology, University of Heidelberg, Im Neuenheimer Feld 153, 69120 Heidelberg, Germany, [3]Central Unit Biostatistics, German Cancer Research Center, Im Neuenheimer Feld 280, 69120 Heidelberg, Germany and [4]Cnopf'sche Kinderklinik, Nürnberg Children's Hospital, St. Johannis Muehlgasse 19, 90419 Nuernberg, Germany

Received October 16, 2006; Revised February 1, 2007; Accepted February 2, 2007

ABSTRACT

Existing microarray-based approaches for screening of DNA methylation are hampered by a number of shortcomings, such as the introduction of bias by DNA copy-number imbalances in the test genome and negligence of tissue-specific methylation patterns. We developed a method designated array-based profiling of reference-independent methylation status (aPRIMES) that allows the detection of direct methylation status rather than relative methylation. Array-PRIMES is based on the differential restriction and competitive hybridization of methylated and unmethylated DNA by methylation-specific and methylation-sensitive restriction enzymes, respectively. We demonstrate the accuracy of aPRIMES in detecting the methylation status of CpG islands for different states of methylation. Application of aPRIMES to the DNA from desmoplastic medulloblastomas of monozygotic twins showed strikingly similar methylation profiles. Additional analysis of 18 sporadic medulloblastomas revealed an overall correlation between highly methylated tumors and poor clinical outcome and identified *ZIC2* as a frequently methylated gene in pediatric medulloblastoma.

INTRODUCTION

DNA methylation has been shown to play an essential role in various physiological processes such as mammalian development (1), genomic imprinting (2), X chromosome inactivation (2) and aging (3). DNA methyltransferases (DNMTs), three of which have been identified in humans to date, are responsible for *de novo* methylation (mainly DNMT1, DNMT3a and DNMT3b) as well as for maintenance of methylation (mainly DNMT1). The importance of these enzymes has been shown in mouse models. Mice deficient in any of the three DNMTs die early in development or immediately after birth (4). Hypomethylation of bulk genomic DNA (5,6) and hypermethylation of CpG islands (CGIs) (7) have been implicated in the initiation and progression of human cancer. Defined as stretches of genomic DNA >500 bp with a G + C content ≥55% and observed CpG:expected CpG dinucleotide ratio of >0.65, CGIs are most frequently encountered in promoter regions or first exons of genes (8), and ~60% of genes harbor a CGI in their 5′ region (9). Hypermethylation of promoter CGIs may lead to transcriptional repression of associated genes, e.g. tumor-suppressor genes (TSGs). Epigenetic silencing is well recognized as a 'third pathway' in Knudson's model of TSG inactivation in cancer, which requires inactivation of both alleles of a gene (10,11). Moreover, as many or even more loci can be subject to hypermethylation as

*To whom correspondence should be addressed. Tel:+49-6221-424619; Fax: +49-6221-424639; Email: m.macleod@dkfz.de
The authors wish it to be known that, in their opinion, the first two authors should be regarded as joint First Authors

are inactivated by mutations in human cancer (11). On the other hand, hypomethylation of promoter sequences may reactivate the expression of silenced oncogenes and hypomethylation of mobile genomic elements leads to chromosomal instability, linking epigenetic and genetic phenomena (12). The methylation status of specific gene promoters could be linked to the pathogenesis of various types of cancer (13), and tumor-specific methylation changes have been established as prognostic markers in many tumor entities (13). Epigenetic events moved into the focus of interest of many researchers and clinicians due to the fact that, unlike genetic modifications such as mutations or genomic imbalances, epigenetic changes are potentially reversible, making them especially interesting therapeutic targets in cancer and other diseases. Demethylating agents such as azacytidine and some of its derivatives are under extensive investigation for clinical application in patients with hematological malignancies (14) as well as in solid tumors (15). In medulloblastoma, no genome-wide approach to study methylation patterns has been conducted to date. However, several genes, such as RASSF1, CASP8 and HIC1, were shown to be frequently hypermethylated in their promoter regions (16–18).

In recent years, different techniques have been developed for genome-wide screening of CGI methylation in normal as well as in diseased tissues. Along with restriction landmark genomic scanning (RLGS) (19) and mass spectrometry (MALDI-TOF) (20) approaches, various DNA microarray-based methods have been established using different microarray platforms [CGI arrays, BAC arrays (21), oligonucleotide arrays (22)] and different procedures for amplicon generation. The first and most widely used method, differential methylation hybridization (DMH), was introduced by Huang and coworkers in 1999 (23). DMH is used to determine the methylation of CGI sequences in a test sample relative to a control sample. Test and control DNA are digested with one or several methylation-sensitive enzyme(s) and only the methylated, and hence uncut, DNA is amplified by linker-mediated PCR. The PCR products are differentially labeled, and hybridized to a CGI microarray. DMH has been used to study aberrant methylation patterns in various tumor entities and cell lines (24,25). DMH typically compares tumor tissue and unrelated control tissue, as the cell type of tumor origin is often unknown or the cell population is too small to obtain sufficient amounts of control DNA. Tissue-specific methylation patterns of unrelated control tissues, however, will likely result in numerous false-positive and false-negative results. Furthermore, DNA copy-number imbalances severely bias the readout of this method, since regions of copy-number gains and losses erroneously appear as hypermethylated and hypomethylated, respectively, if methylation-sensitive restriction is incomplete.

A variation of the DMH technique proposed by Adrien *et al.* (26) uses isoschizomeres to perform a methylation-sensitive and methylation-insensitive digestion at the same restriction site. Although this method theoretically overcomes problems of genomic imbalances and tissue-specific methylation patterns, the approach has a principal weakness in that unmethylated sequences will not give a fluorescence signal at all since they will be cut by both enzymes and will therefore not be amplified in the following PCR.

More recently, methylated DNA immunoprecipitation (MeDIP) and methylated-CGI island recovery assay-assisted microarray analysis (MIRA) were introduced as alternative methods for the enrichment of methylated DNA (27,28). Although being an elegant alternative for some applications, the major disadvantage of the MeDIP assay is the large amount of template DNA required (minimum 4 μg), which is often not feasible for clinical applications. If an amplification step is included, PCR bias is introduced due to the fact that 'precipitate' (enriched in methylated CGIs) and 'cleared input' (genomic DNA not enriched for CGIs) significantly differ in their GC content and thereby in their performance during PCR amplification.

McrBC, the methylation-specific enzyme used for array-based profiling of reference-independent methylation status (aPRIMES), has initially been used in methylation studies to remove methylated sequences from genomic DNA and to map methylated sites, e.g. on metaphase chromosomes (29–31). Later it has also been incorporated in a micorarray-based methylation profiling approach (32).

To overcome some of the limitations of established methods, we developed a novel technique designated aPRIMES for genome-wide detection of CGI methylation status, which is independent of a control tissue.

MATERIALS AND METHODS

Tumor material and patient characteristics

Tumor samples were collected by W. Scheurlen at the Department of Pediatric Oncology, Wuerzburg University Hospital (Wuerzburg, Germany) and Department of Pediatric Oncology, Mannheim University Hospital (Mannheim, Germany), between 1994 and 2002. All diagnoses were confirmed by histological assessment of specimens obtained at neurosurgery by at least two neuropathologists according to the criteria of the World Health Organization (WHO) classification. Approval to link histological data to clinical data was obtained by the Institutional Review Board. This procedure is according to the official statement of the National Ethics Council of the Federal Government of Germany (March 2004). Staging procedures included MRI before and immediately after neurosurgery. Metastatic disease was detected by craniospinal imaging and lumbar puncture. Patients were treated according to German standard therapy protocols of the HIT study group. Genomic DNA from normal cerebellum (pool of five donors, age 25–33 years) was purchased from Biocat (Heidelberg, Germany).

Nucleic acid isolation

Extraction of high molecular weight DNA and RNA from frozen medulloblastoma samples was carried out by ultracentrifugation in cesium chloride as previously described (46). Total RNA quality and concentration was controlled

with the Agilent 2100 bioanalyzer (Agilent Technologies, Palo Alto, USA).

CGI library and probe preparation

A human library consisting of 10 560 bacterial clones harboring DNA sequences enriched for CGIs was purchased from the UK HGMP (http://www.hgmp.mrc.ac.uk/). This clone set is part of the original CGI library which was generated by Cross *et al.* (33). To amplify CGI sequences, library aliquots were grown in 1 ml LB media plus ampicillin (50 µg/ml) overnight at 37°C. PCR was performed in a 96-well format (MWG, Ebersberg, Germany) using 2 µl of bacterial culture supplemented with 10% DMSO, 180 µM dNTPs, 150 nM of each primer, 1.8 mM $MgCl_2$ and 2U Eurotaq Polymerase (Biocat, Heidelberg, Germany). Thirty-five amplification cycles were performed including denaturing at 94°C for 30 s, annealing at 58°C for 30 s and elongation at 72°C for 60 s. Primers used for amplification were pGEM-for (5′-GGCCGCGGGATATCACTA-3′) and pGEM-rev (5′CTCAAGCTATG CATCCAACG-3′). All CGI sequences were reamplified by using 5 µl of product of the first PCR as a template for a second PCR under identical conditions. The second PCR resulted in more homogenous product quantities for microarray printing.

CGI microarray production

For microarray printing, 30 µl of PCR products was dried in a vacuum centrifuge and resuspended in 12 µl spotting buffer (3 × SSC, 1.5 M betaine). PCR products were printed onto amino-silane-coated Corning™ Gaps II slides (Corning, Acton, USA) in triplicates using a printing robot (OmniGrid, GeneMachines, San Carlos, USA) and 48 (4 × 12 configuration) Telechem SMP3 pins (Telechem International, Sunnyvale, USA) at 20°C and 40% humidity. After printing, slides were UV cross-linked, baked for 2 h at 80°C, and UV cross-linked again.

aPRIMES

Here, 500 ng genomic DNA was restricted to completion with 10 U MseI for 3 h in a final volume of 10 µl in the buffer provided by the supplier (New England Biolabs, Beverly, USA). Heat inactivation was carried out at 65°C for 20 min. MseI fragments were then subjected to linker-mediated PCR as essentially described by Klein and coworkers (47). Briefly, 1 µl each of 100 µM stock solution (MWG, Ebersberg, Germany) ddMse11 (5′-TAA CTGACAG-3′) and Lib1 (5′-AGTGGGATTCCTGCTG TCAGT-3′) were annealed in 1 µl One-Phor-All-Buffer and 3 µl ddH_2O. Annealing was started at a temperature of 65°C and was shifted down to 15°C with a ramp of 1°C/min. At 15°C, 10 µl MseI fragments, 2 µl of ATP (10 mM) and 2 µl T4-DNA-Ligase (10 U; Roche, Grenzach-Wyhlen, Germany) were added, and primers and DNA fragments were ligated overnight.

Half of the resulting ligated MseI fragments were digested with the restriction enzyme McrBC (New England Biolabs, Beverly, MA, USA) for 8 h following the conditions recommended by the supplier. The other half of the MseI fragments was digested with the two methylation-sensitive endonucleases HpaII (New England Biolabs; recognition site CCGG, 3 h, 37°C) and BstUI (New England Biolabs; recognition site CGCG, 3 h, 60°C) according to the recommendations of the supplier. Digested DNA fragments were then treated with 1 µl Proteinase K (Invitrogen, Karlsruhe, Germany) for 1 h at 37°C with subsequent heat inactivation at 80°C for 10 min.

For the following amplification step, 10 µl consisting of 2 µl 10 × Expand Long Template buffer 1 (Boehringer, Mannheim, Germany), 1 µl dNTPs (10 mM), 1 µl Lib1 primer (5′-TAACTAGCATGC-3′), 1 µl expand long template DNA polymerase mixture (Boehringer, Mannheim, Germany) and 5 µl ddH_2O were added to 20 µl reaction volume. A MWG thermocycler was programmed to 72°C for 3 min, followed by 20 cycle loops at 94°C (30 s), 62°C (30 s) and 72°C (90 s). Final elongation was carried out at 72°C for 10 min. PCR products were recovered by ethanol precipitation. DNA was eluted in 30 µl 0.1 × TE, pH 8.

Labeling and hybridization to microarrays

Labeling, hybridization and washing procedures were adapted from a previously published protocol (48). Briefly, 13 µl of both the McrBC-digested and the HpaII/BstuI-digested samples of each tumor were differentially labeled with Cy3- or Cy5-conjugated dCTP by use of a BioPrime DNA Labeling Kit (Invitrogen, Karlsruhe, Germany). Here, 75 µl (~10 µg) each of McrBc and Hpa/BstUI samples were combined with 150 µg human Cot-1 DNA (Roche Diagnostics, Mannheim, Germany) to block repetitive sequences. Unincorporated nucleotides, random primers and dyes were removed by ethanol precipitation. Precipitated DNA was resuspended in 135 µl Ultrahyb™ hybridization buffer (Ambion, Bad Soden, Germany). Denaturation of samples was performed at 75°C for 10 min, followed by re-annealing at 37°C for 30 min. Hybridization was carried out in a GeneTAC Hybridization Station (Genomic Solutions, Oberhaching, Germany) for 40 h at 37°C. Slides were washed with 2 × SSC/0.05% Tween-20 at 37°C for 1 cycle, 2 × SSC/0.05% Tween-20 at 44°C for 2 cycles, 50% formamide/2 × SSC/0.1% Tween-20 at 44°C for 3 cycles, 2 × SSC/0.05% Tween-20 at 44°C for 2 cycles, and finally 1 × PBS/0.05% Tween-20 at 25°C for 2 cycles. Slides were dried by centrifugation at 216 g for 3 min in a clinical centrifuge.

Image and microarray data analysis

Arrays were scanned with an Agilent DNA microarray scanner (Agilent Technologies, Palo Alto, USA) and images analyzed using GenePix Pro 6.0 software (Axon Instruments, Burlingame, USA). Fluorescence intensities of all spots were filtered consistently (intensity/local background >1.1; mean/median intensity <0.25; coefficient of variation of log_2-ratios between replicated spots >0.3 if range of log_2-ratios of replicated spots >0.2). Global normalization was performed in three steps. First, we applied a normalization for print-order effects using the loess smoother, as described in Smyth *et al.* (49). In

the second step, within-array normalization was done to normalize the $\log_2$-ratios for each array separately by the use of print-tip loess (49). Third, to normalize between arrays, quantile normalization was performed as described by Yang and Thorne (50). Normalization was carried out using zero weights for previously filtered spots. The data sets discussed in this publication have been deposited in NCBIs Gene Expression Omnibus (http://www.ncbi.nlm.nih.gov/geo/) and will be accessible through GEO Series accession number GSE4857 after publication of this article.

Internal controls

Spike CGIs from rice were used as positive controls for methylation. Ten rice CGIs were PCR amplified and printed on the microarray. Sample DNAs for aPRIMES were spiked with ~10 pg of each *in vitro* methylated rice CGI. Mitochondrial CGI clones present in the original library were used as controls for unmethylated and allelically/partially methylated CGIs.

Sequence information of candidate CGIs

Sequence information for CGI clones was obtained from a publicly available database at http://data.microarrays.ca/cpg/index.htm. Chromosomal annotation of sequences is based on the University of California at Santa Cruz (UCSC) genome database (Freeze, May 2004). Here, 150 clones from the CGI library, including the two clones representing the ZIC2 promoter region, were sequenced with the same primers as used for amplification.

Bisulfite conversion and pyrosequencing

Here, 500 ng of patient-sample-derived DNA was bisulfite-converted according to standard protocols. The modified DNA was subjected to PCR amplification and subsequent pyrosequencing. Primer sequences for the PCR amplification were F_102212_zic2: 5′-GGGATTTTTTGGTTTTTGAAGA-3′ and R_102212_zic2: 5′- Biotin-AACCACAAAACCCACAACTATC-3′. Amplification was carried out after an initial denaturation step (94°C, 3 min) for 50 cycles of 30 s at 94°C, 30 s at 54°C and 45 s at 72°C in a final volume of 50 µl. Final extension was performed for 5 min at 72°C. *In vitro* methylated DNA from peripheral blood mononuclear cells of healthy donors was used as a positive control for the methylated status (IVM). *In vitro* methylation was carried out using SssI *in vitro* methylase (New England Biolabs, Beverly, USA) for 4 h according to the manufacturer's instructions.

Here, 30 µl of PCR product was immobilized to 3 µl Streptavidin Sepharose™ HP beads (GE Healthcare, formerly Amersham Biosciences) followed by annealing to 4 pmol sequencing primer for 2′ at 80°C. Sequencing primers were S1_102212_zic2 (5′-GTTTTTGAAGATAATTTTAAT-3′) for CpG 1-5 and S2_102212_zic2 (5′-GGTTTTGAGTTGGATT) for CpG 6-12. The analysis criteria were those specified by the manufacturer's settings. CpG analysis were done with Pyro Q-CpG software.

QRT-PCR

To correlate the methylation status of *ZIC2* with mRNA expression, 5 µg of total RNA from tumor samples and normal human cerebellum (pool of 24 individuals, aged 16–70; BD Biosciences, San Jose, USA) as a reference was used as a template for reverse transcription with the SuperscriptII first-strand synthesis kit (Invitrogen, Karlsruhe, Germany). Each cDNA sample was analyzed in triplicate using ABI PRISM 7700 (Applied Biosystems, Foster City, USA) with Absolute SYBR Green ROX Mix (ABgene, Epsom, UK) according to the manufacturer's instructions. Two endogenous housekeeping genes (*PGK1*, *LMNB1*) were used for internal normalization. All primers were tested to exclude amplification from genomic DNA. Quantification of the transcript of interest relative to the housekeeping genes was calculated according to a previously published algorithm (51). Oligonucleotide sequences for ZIC2 were for 5′-TCCGAGAACCTCAAGATCC and rev 5′-TAGGGCTTATCGGAGGTG.

RESULTS

Methylation analysis using aPRIMES

Array-PRIMES compares two differentially restricted aliquots from the same genome of interest by competitive hybridization to a CGI array. By performing a test-versus-test rather than test-versus-control hybridization, influences of tissue-specific methylation patterns in the control DNA as well as of DNA copy-number imbalances that might be present in the test, but not in the control genome, are avoided. Due to amplification of whole genomic DNA in both parts of the sample, no PCR bias is introduced. The flowchart of our newly developed protocol is depicted in Figure 1a. Briefly, genomic (tumor) DNA is digested with MseI and ligated to adapter primers. Subsequently, one-half of the sample is digested with the methylation-sensitive restriction enzymes HpaII and BstUI to cut unmethylated CGIs, and the remaining half is digested with the methylation-specific enzyme McrBC to cut methylated CGIs. Since the probability of a McrBC recognition sequence ($5'\ldots Pu^mC[N_{40-3000}]Pu^mC\ldots 3'$) to be present within a CGI is close to 100%, and the probability for either a HpaII or BstUI site was found to be ~90% in the 150 clones that we have sequenced, the vast majority of clones on the CGI microarray are potentially informative. Restricted samples are then subjected to 20 cycles of linker-mediated PCR, differentially labeled with fluorescent dyes, and competitively hybridized to a CGI microarray. The microarray used for this study consists of 10 560 sequences enriched for CGIs as obtained by isolation over a MeCP2 (methyl-CpG-binding protein 2) affinity column by Cross and coworkers (33), 595 PCR products of interest representing regions of frequent genomic losses in medulloblastoma that might harbor yet-unidentified TSGs, and 10 CGIs from rice that can be used to spike the test DNA. Rice DNA was chosen to rule out cross-hybridization with human CpG-rich sequences.

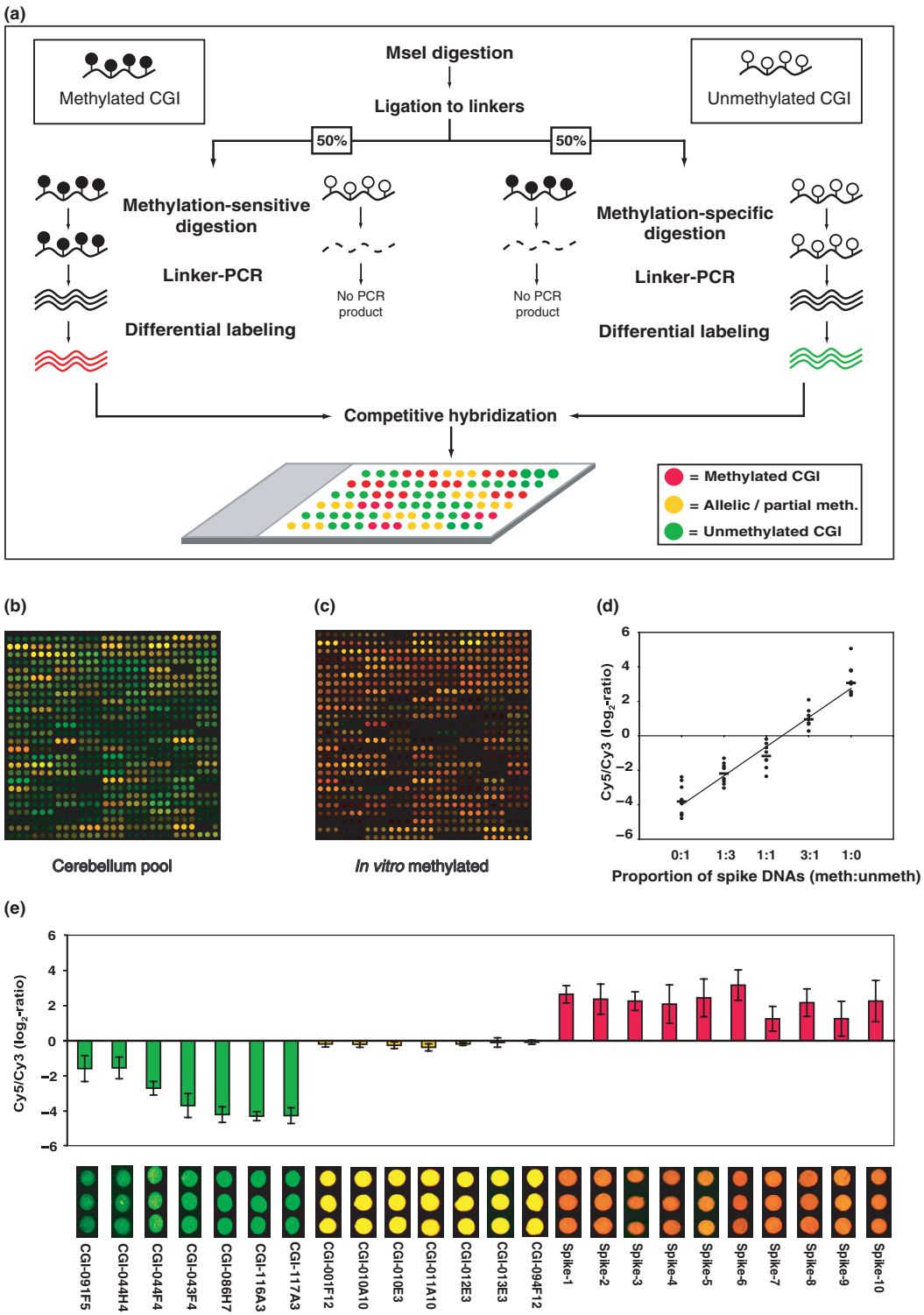

Figure 1. Flowchart for the array-PRIMES procedure and performance of the method. (**a**) Flowchart and overview of expected results for methylated and unmethylated CGIs. (**b** and **c**) Performance of aPRIMES on CGI microarrays. All clones are spotted in triplicate. A representative block is shown for (**b**) normal cerebellum (pool of five unaffected donors) and (**c**) *in vitro* methylated tumor DNA. Red spots indicate methylated clones, green spots indicate unmethylated clones, yellow spots indicate mixed or allelic methylation, and can also be caused by a lack of appropriate restriction sites. (**d**) Quantification of methylation of spike CGIs using different proportions of methylated and unmethylated spike DNA spiked into genomic DNA of one tumor. Spots indicate the normalized ratios of all eight spike clones used in each of five experiments; short horizontal lines represent the median ratio of eight clones. The regression line is based on the medians depicted in the diagram. (**e**) Performance of internal control clones. Median values and median absolute deviations from the median (MADs) of 20 unselected aPRIMES experiments (upper part) and spot data from one representative hybridization (lower part) are shown. Methylated clones are highlighted in red and are expected to result in positive ratios; mitochondrial clones with methylation-sensitive restriction sites are highlighted in green and are to have negative ratios. Mitochondrial clones without methylation-sensitive restriction sites are depicted in yellow and are to be balanced.

To test the performance of aPRIMES, we analyzed CGI methylation in 20 pediatric medulloblastomas and normal cerebellum (pool of five unaffected donors, age 25–33 years). A representative section of a CGI microarray hybridized with cerebellum pool DNA is shown in Figure 1b. Most clones indicate an unmethylated state (green spots), some clones are clearly methylated (red), whereas most of the remaining spots show a faint or even absent fluorescence signal. This result is obtained whenever restriction sites for methylation-sensitive and methylation-specific enzymes are both present in each copy of the respective DNA stretch. In a typical aPRIMES experiment, ~20% of all clones are filtered out due to this reason during data processing. Yellow spots are not as frequent and represent a balanced status. This can be caused by various scenarios: allelic methylation, differential methylation in subsets of tumor cells or unmethylated clones lacking a methylation-sensitive restriction site (HpaII or BstUI). *In vitro* methylated tumor DNA was used as a positive control to detect the proportion of clones that can potentially be methylated (Figure 1c). The vast majority of clones (>90%) indicate a methylated status in these experiments. The reproducibility of the method is excellent. Spearman correlation coefficients (r) for the correlation of normalized results are typically >0.90 (Supplementary Figure 1 online).

To verify that aPRIMES detects the direct methylation status of a given CGI, we performed five experiments with DNA from the same tumor and spiked different proportions of methylated:unmethylated DNA (0:1, 1:3, 1:1, 3:1 and 1:0) from eight rice CGIs into the tumor DNA. Figure 1d illustrates that aPRIMES accurately detects quantitative differences in the percentage of methylated DNA.

For internal validation of each experiment, we used a set of 24 control clones reflecting the different states of methylation: 14 clones derived from mitochondrial DNA that were part of the clone library and 10 CGI clones from rice (Figure 1e). Mitochondrial DNA is known to be unmethylated *in vivo* (34). Therefore, mitochondrial CGIs represent the unmethylated state (appearing green on the microarray) when containing a methylation-sensitive restriction site (clones CGI-091F5 to CGI-117A3), or the balanced state (yellow) if no methylation-sensitive restriction site is present (CGI-001F12 to CGI-094F12). In the latter case, none of the applied enzymes is effective, and DNA is amplified in both, the methylation-sensitive and methylation-specific restriction aliquots. As a control for the methylated state, 10 CGIs from rice represented on the CGI array (Spike-1 to Spike-10) were *in vitro* methylated and spiked into the tumor DNA prior to enzymatic restriction. The median ratio over all 20 aPRIMES analyses of medulloblastomas and the typical appearance on the hybridized CGI array are shown for each of the 24 control clones (Figure 1e). In all three control groups, the correct methylation status was indicated by all clones, including those with low signal intensities.

Global CGI methylation in medulloblastomas from monozygotic twins and sporadic cases

Two of the analyzed medulloblastomas were derived from monozygotic twins presenting with desmoplastic medulloblastoma at three years of age. Analysis of DNA copy-number by array-CGH (median resolution ~0.4 kb) showed that none of the tumors carried chromosomal aberrations (data not shown). CGI methylation analysis by aPRIMES, however, clearly showed aberrant methylation of the tumor genomes compared to normal cerebellum, indicating that aberrant DNA methylation is involved in the pathogenesis of the twins' tumors (Figure 2a). Interestingly, the epigenomes of the tumors were strikingly similar to one another (Figure 2b), but quite different from that of an unrelated sporadic tumor (Figure 2c), suggesting that the twin's tumors share a unique epigenetic pathomechanism.

Comparison of methylation patterns between tumors revealed considerable variability in the overall degree of CGI methylation. For example, many more clones were methylated in medulloblastoma M5 than M1 (Figure 2c, upper left quadrant). Representative sections of the arrays of both patients are given in Figure 2d and e. Examples for clones methylated in M5 and unmethylated in M1 are highlighted with white circles. These differences in global methylation prompted us to compare the percentage of highly methylated clones in a set of 20 medulloblastoma samples. For this purpose, we determined the median absolute deviation from the median (MAD) as a robust estimate of the true standard deviation over all clones present in at least 50% of experiments after consistent filtering for each sample. Clones with $\log_2$-ratios of more than two MADs above the median were assumed to be highly methylated. When applying this threshold to the validation experiment shown in Figure 1d, only two of the spike CGIs with a methylated:unmethylated proportion of 3:1 will be regarded as highly methylated, whereas all fully methylated spike CGIs will. Based on this conservative threshold, we grouped the 20 patients (including the twins) into two equally large groups according to the percentage of highly methylated clones. Concerning histological subtypes, both groups are comparable: The low methylator group contains three patients with desmoplastic tumors (one in the high methylator group) and one patient with anaplastic tumor (none in the high methylator group); the remaining cases are classic medulloblastomas. The groups are also comparable with regard to patient age (mean 6.1 versus 6.7 years), gender (five male versus five female patients in both groups) and therapy regimen (three versus two patients were 2 years or younger and were therefore not subjected to radiotherapy). Patients in the low methylator group have 8.9% or less of highly methylated clones (range: 6.2–8.9%, 10 patients). The remaining 10 patients were grouped into a high methylator group having 9% or more highly methylated clones (range 9–11.2%). Interestingly, patients in the low methylator group had a better prognosis than patients in the high methylator group in this series. The median overall survival was 52 and 84 months in the low and high methylator groups, respectively. Whereas only 1/10

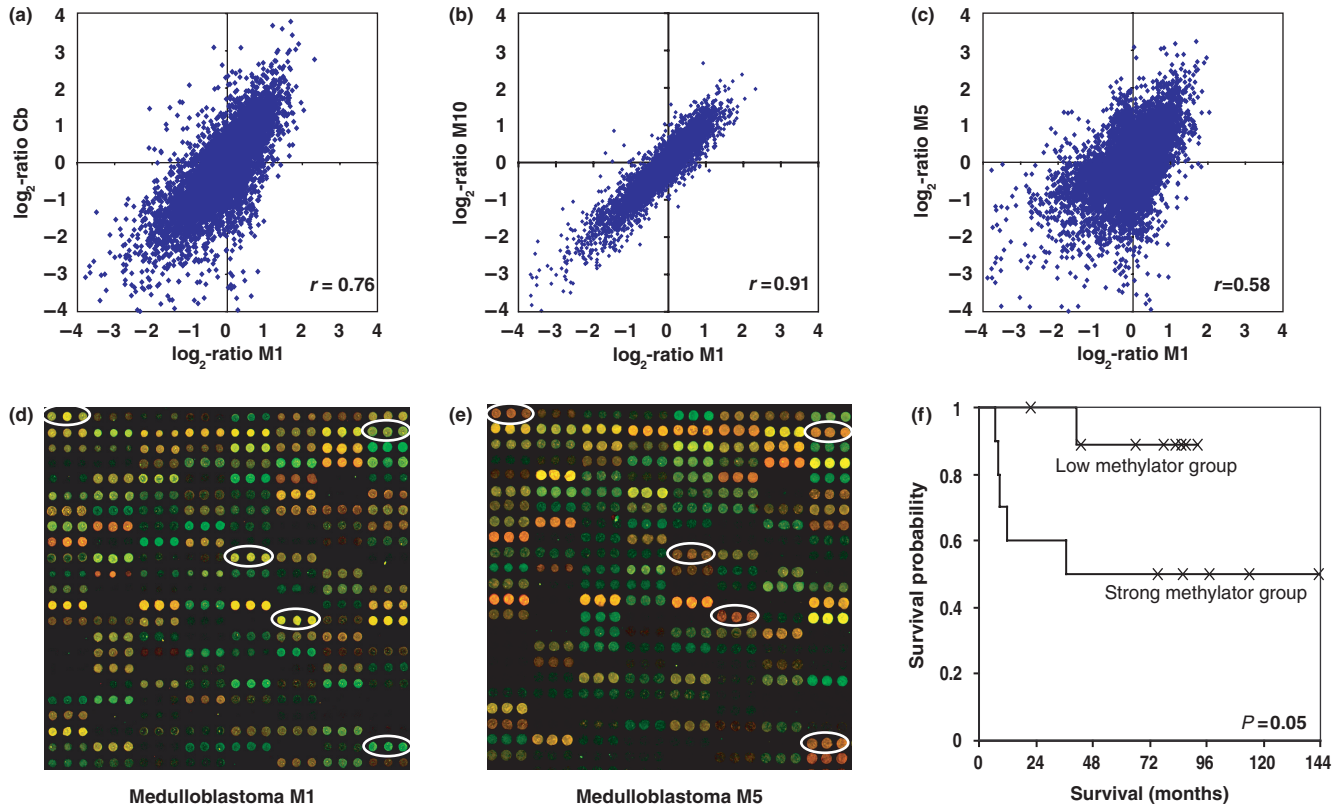

Figure 2. Application of aPRIMES in pediatric medulloblastoma identifying groups with low and high methylation. (**a–c**) Scatter plots representing the correlation of methylation patterns of monozygotic twins (patients M1 and M10) with simultaneous desmoplastic medulloblastoma, a case of sporadic classic medulloblastoma (M5), and normal cerebellum. (**a**) twin one (patient M1) in comparison with normal cerebellum (pool of five unaffected donors), (**b**) twin 1 versus twin 2 (patient M10) and (**c**) twin one compared with a sporadic classic medulloblastoma (patient M5). Spearman-correlation coefficients (r) are given for each plot. Representative microarray sections of (**d**) patient M1 (low methylator group) and (**e**) patient M5 (high methylator group). Examples for differentially methylated clones are highlighted with white circles. (**f**) Kaplan–Meier plot of estimated survival time distribution with corresponding log-rank test. For survival analysis, patients were grouped into low and high methylator groups according to the percentage of highly methylated clones.

patients died in the first group, 5/10 patients died in the high methylator group after a median follow-up of 79 months. The Kaplan–Meier plot (Figure 2f) shows the estimated survival probability of the two groups (log-rank-test: $P = 0.05$). Furthermore, the global methylation status is not associated with the frequency of copy-number alterations in the tumor genome. For example, the tumor displaying the highest percentage of methylated clones shows a balanced tumor genome as assessed by array-based comparative genomic hybridization (data not shown).

ZIC2 is differentially methylated and epigenetically silenced in pediatric medulloblastoma

For the identification of candidate clones, highly repetitive sequences (repeat content >50% according to the UNH database at www.data.microarrays.ca/cpg/) were excluded. We next sorted individual clones according to their MAD to screen for differentially methylated clones within the series of medulloblastomas. Two of the most differentially methylated clones were CGI-027A11 and CGI-028A11 representing the CGI of the zinc-finger protein of the cerebellum family member 2 (*ZIC2*) gene. Clone identities were confirmed by DNA sequencing (data not shown). The predicted CGI within the MseI fragment is depicted in Figure 3a. The methylation status of *ZIC2* in 20 medulloblastomas as well as in appropriate positive and negative controls was assessed by pyrosequencing of the region indicated in Figure 3a covering 12 individual CpG sites (Figure 3b, grey bars and Supplementary Figure 2). The percentages indicated in Figure 3b reflect the median methylation of all investigated CpG dinucleotides for each sample. Confirming the results obtained by aPRIMES, the signal ratios from the microarray experiments show an excellent correlation with the pyrosequencing results (Spearman correlation $\rho = 0.89$). Differences between the readout obtained by pyrosequencing and aPRIMES (mainly tumors M6, M12, M17 and M18) may well be explained by additional methylation sites outside the pyrosequencing region. To further assess the functional impact of this methylation event, we measured mRNA expression in tumors, of which RNA was available using quantitative real-time PCR. Notably, we found silencing of mRNA expression in most medulloblastoma samples when normalized to a pool of normal cerebellum in two independent experiments, corroborating the results of our methylation analyses (Figure 3c). The downregulation of mRNA expression in tumor M4 cannot be explained by

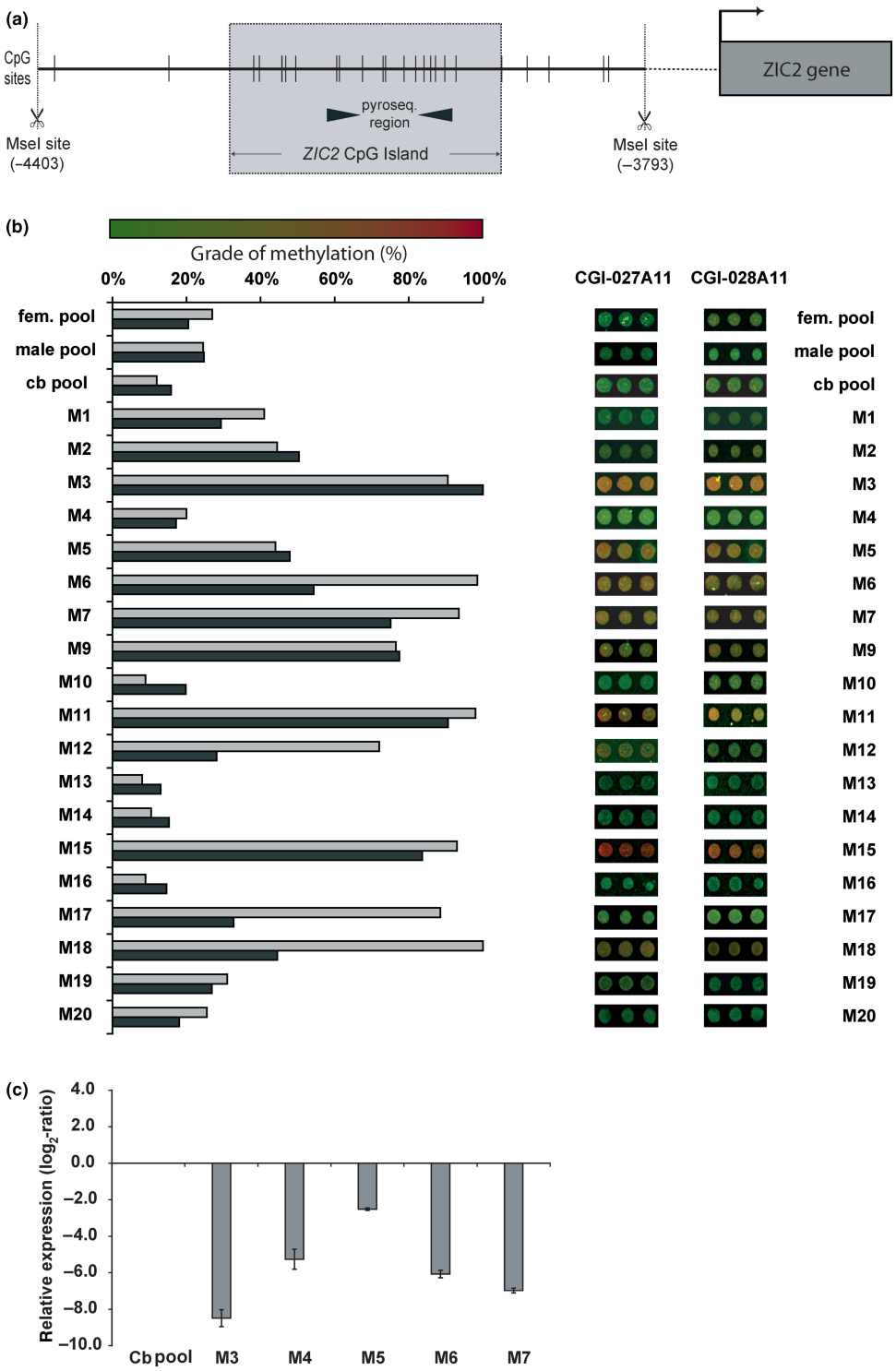

Figure 3. CGI methylation and mRNA expression of *ZIC2* in pediatric medulloblastoma. (**a**) Schematic presentation of the predicted *ZIC2* CpG island in the 5' UTR of the gene (chr13: 99428130-99428406) delineated according to the criteria by Gardiner-Garden and Frommer (52). MseI-sites flanking the ends of the CGI clone are shown together with their position in relation to the transcription start site. Pyrosequencing was performed for the indicated region. (**b**) Comparison between pyrosequencing results (grey bars) and aPRIMES results (black bars). For comparison, aPRIMES ratios were linearized and are given in relation to the linear ratio of tumor M3 that displayed the highest ratio among all aPRIMES samples, and was therefore set to 100%. For the pyrosequencing data, a median over all 12 investigated individual CpG sites was calculated. The right panel illustrates non-normalized spot-data after performance of aRPIMES. Triplicate spots for both ZIC2 clones, namely CGI-027A11 and CGI-028A11 are indicated Fem. (male) pool = DNA derived from the peripheral blood mononuclear cells (PBMCs) of 10 healthy donors below age 35. Cb pool = pool of cerebellum DNA from five unaffected donors, age 25–33 years. M1–M20: pediatric medulloblastoma samples. For medulloblastoma M8 no chip data are available. (**c**) mRNA abundance of *ZIC2* was assessed by quantitative real-time PCR and normalized to the expression of *ZIC2* in a cerebellum mRNA pool of 24 unaffected individuals. Medians and MADs of two independent experiments are shown. *ZIC2* was downregulated to different degrees in all tested medulloblastomas, most profoundly in tumor M3 that displayed the highest methylation of the CGI.

CGI methylation, and may be caused by other mechanisms of transcriptional regulation.

DISCUSSION

This study demonstrates that aPRIMES allows for genome-wide detection of the direct methylation status of individual DNA fragments with high accuracy and reproducibility. Major limitations of established methods (21,23) are overcome by comparative hybridization of differentially restricted fractions of one test genome making the procedure independent of a control tissue. In contrast to other approaches including those based on immunoprecipitation of methylated DNA (22,27,32), aPRIMES can distinguish between unmethylated, partially or allelically methylated, and fully methylated clones. Furthermore, PCR bias is avoided due to amplification of total genomic DNA in both samples rather than GC enriched versus total genomic DNA as required for MeDip in clinical applications (27). In contrast to the method proposed by Nouzova *et al.* (32), which was the first microarray-based method to be independent of a common reference, aPRIMES data can be normalized by commonly used algorithms (loess, vsn) because values display a symmetric distribution around the balanced state. Equal distribution of unmethylated and methylated sequences may increase sensitivity to detect differential methylation. In addition, aPRIMES can distinguish partial and full methylation. Recently, another microarray-based method for global methylation profiling was developed, termed microarray-based methylation assessment of single samples (MMASS) (35). This method is comparable to aPRIMES in that it makes use of differential restriction of the test genome. In contrast to Ibrahim *et al.* (35) aPRIMES allows the quantification of methylation signals and between-chip normalization by use of 24 internal control fragments representing the different states of methylation.

We applied aPRIMES to a series of 20 pediatric medulloblastomas including tumors from 3-year-old twins with simultaneous desmoplastic medulloblastoma. Previously, it was found that differences in the epigenomes of monozygotic twins are mostly acquired with aging (36). To our knowledge, this is the first report on the similarity of tumor epigenomes in monozygotic twins presenting with a tumor of the same entity. While no gross genomic imbalances could be detected, differences between the methylation patterns of the twins and normal cerebellum are demonstrated, indicating that aberrant methylation is involved in the pathogenesis of the tumors. These results suggest a shared epigenetic pathogenesis of the tumors.

Analysis of the methylation profiles of 20 pediatric medulloblastomas revealed large differences in the proportion of highly methylated CGIs. Therefore, we grouped the patients into two equally large groups according to the proportion of methylated clones and found that patients in the high methylator group had a worse prognosis. Obviously, this result has to be validated prospectively in a larger series of tumors. However, the fact that grouping is independent of the number of genomic imbalances, histological subtype, age, gender and treatment regimen makes this result a very promising basis for further exploration. Notably, the continuous distribution of methylation frequency obtained in this study using unselected clones, argues against the existence of a CGI methylator phenotype (CIMP) in medulloblastoma. CIMP is characterized by a high degree of concordant CGI methylation in a subset of tumors of a certain entity and was first described by Toyota *et al.* (37) as a distinct pathway for colorectal carcinogenesis. CIMP suggests that there should be two clearly disparate groups of methylation frequency in a given tumor cohort, which is not the case in the cohort analyzed here. It is important to note, however, that the concept of CIMP is entirely based on studies with relatively small sets of pre-selected CGI clones. Therefore, it will be of great interest to carry out genome-wide methylation studies with unselected clones in larger tumor series.

Based on robust statistical analysis, two clones representing the *ZIC2* CGI were among the most differentially methylated clones within the investigated series of pediatric medulloblastomas. Differential methylation was validated by methylation-specific PCR, and marked silencing of mRNA expression upon CGI methylation was demonstrated by use of quantitative real-time PCR. *ZIC2* is an interesting candidate gene in medulloblastoma for several reasons. *ZIC2* belongs to a family of five ZIC genes that encode zinc-finger transcription factors, each of which is composed of five Cys_2His_2 zinc-finger domains. In mice, the *ZIC* genes were shown to be essential for a wide variety of developmental processes, such as central nervous system, muscle and skeletal development, and the embryonal establishment of left–right asymmetry (38). In humans, heterozygous deletions or mutations in the *ZIC2* gene, along with mutations in the Sonic Hedgehog (*SHH*) gene and others, are found in subsets of patients with holoprosencephaly (HPE), a congenital malformation of the forebrain with a very diverse phenotypic spectrum, including non-separation of the two hemispheres and facial dysmorphisms (39). In medulloblastoma, expression of *ZIC* genes was identified as an indicator that cerebellar granule cells might be the cells of origin for this tumor entity (40). Recently, it has been shown that the neuronal cell-type-specific promoter of the α CaM kinase II (*CamKII*) gene is activated by ZIC2 (41). CaMKII in turn was shown to be responsible for the phosphorylation and inactivation of the proto-oncogene ETS1, and to antagonize wnt/β-catenin signaling either by direct phosphorylation and inactivation of β-catenin or by blocking TCF/LEF via TAK1/NLK (42,43). In addition, ZIC proteins interact with gli proteins, which function as downstream effectors of the SHH pathway. Interestingly, the expression of ZIC family proteins grossly overlaps with expression of the repressing Gli3 in neural tube development (44). The genomic locus of ZIC2 at chromosomal band 13q32 is frequently lost in pediatric medulloblastoma as assessed by array-CGH (19/102 cases; Mendrzyk *et al.* (45) and data not shown). Given the frequent downregulation of ZIC2 in medulloblastoma by aberrant methylation of its promoter and the proposed functions of the ZIC2

protein, our findings suggest an important role for *ZIC2* in the pathogenesis of pediatric medulloblastoma.

In summary, aPRIMES will be useful as a screening tool to identify genes regulated by DNA methylation, such as in epigenetic reprogramming during embryogenesis, tissue-specific gene expression, imprinting and differential gene expression in cancer and other diseases.

SUPPLEMENTARY DATA

Supplementary Data are available at NAR Online.

ACKNOWLEDGEMENTS

We gratefully thank Leonore Senf for the collection and maintenance of the brain tumor bank in the department of W. Scheurlen. Stefanie Hofmann, Magdalena Schlotter and Sibylle Ohl are acknowledged for excellent technical assistance and Daniel Mertens for helpful discussions. Grischa Toedt, Nico Delhomme and Frederic Blond provided valuable bioinformatic support. S.P. is funded by a 'Young Investigator Award' fellowship from the Medical Faculty of Heidelberg, Germany. This work was supported in part by grants of the Bundesministerium für Bildung und Forschung (01 GR 0417 to P.L. and B.R.) as well as the EU MolTools project (LSHG-CT-2004-503155 to P.L.). Funding to pay the Open Access publication charge was provided by the German Cancer Research Center Heidelberg.

Conflict of interest statement. None declared.

REFERENCES

1. Okano,M., Bell,D., Haber,D. and Li,E. (1999) DNA methyltransferases Dnmt3a and Dnmt3b are essential for de novo methylation and mammalian development. *Cell*, **99**, 247–257.
2. Li,E. (2002) Chromatin modification and epigenetic reprogramming in mammalian development. *Nat. Rev. Genet.*, **3**, 662–673.
3. Ahuja,N., Li,Q., Mohan,A., Baylin,S. and Issa,J. (1998) Aging and DNA methylation in colorectal mucosa and cancer. *Cancer Res.*, **58**, 5489–5494.
4. Robertson,K. (2002) DNA methylation and chromatin – unraveling the tangled web. *Oncogene*, **21**, 5361–5379.
5. Feinberg,A. and Vogelstein,B. (1983) Hypomethylation distinguishes genes of some human cancers from their normal counterparts. *Nature*, **301**, 89–92.
6. Ehrlich,M. (2002) DNA methylation in cancer: too much, but also too little. *Oncogene*, **21**, 5400–5413.
7. Baylin,S.B. and Herman,J.G. (2000) DNA hypermethylation in tumorigenesis: epigenetics joins genetics. *Trends Genet.*, **16**, 168–174.
8. Takai,D. and Jones,P.A. (2002) Comprehensive analysis of CpG islands in human chromosomes 21 and 22. *Proc. Natl. Acad. Sci. USA*, **99**, 3740–3745.
9. Antequera,F. and Bird,A. (1993) Number of CpG islands and genes in human and mouse. *Proc. Natl. Acad. Sci. USA*, **90**, 11995–11999.
10. Knudson,A. (2000) Chasing the cancer demon. *Annu. Rev. Genet.*, **34**, 1–19.
11. Jones,P. and Baylin,S. (2002) The fundamental role of epigenetic events in cancer. *Nat. Rev. Genet.*, **3**, 415–428.
12. Feinberg,A.P. (2004) The epigenetics of cancer etiology. *Semin. Cancer Biol.*, **14**, 427–432.
13. Das,P. and Singal,R. (2004) DNA methylation and cancer. *J. Clin. Oncol.*, **22**, 4632–4642.
14. Daskalakis,M., Nguyen,T., Nguyen,C., Gildberg,P., Kohler,G., Wijermans,P., Jones,P. and Lubbert,M. (2002) Demethylation of a hypermethylated P15/INK4B gene in patients with myelodysplastic syndrome by 5-Aza-2′-deoxycytidine (decitabine) treatment. *Blood*, **100**, 2957–2964.
15. Strathdee,G. and Brown,R. (2002) Epigenetic cancer therapies: DNA methyltransferase inhibitors. *Expert Opin. Investig. Drugs*, **11**, 747–754.
16. Lusher, M.E., Lindsey, J.C., Latif, F., Pearson, A.D.J., Ellison, D.W. and Clifford, S.C. (2002) Biallelic epigenetic inactivation of the RASSF1A tumor suppressor gene in medulloblastoma development. Cancer Res., **62**, 5906–5911.
17. Zuzak,T.J., Steinhoff,D.F., Sutton,L.N., Phillips,P.C., Eggert,A. and Grotzer,M.A. (2002) Loss of caspase-8 mRNA expression is common in childhood primitive neuroectodermal brain tumour/medulloblastoma. *Eur. J. Cancer*, **38**, 83–91.
18. Rood,B.R., Zhang,H., Weitman,D.M. and Cogen,P.H. (2002) hypermethylation of HIC-1 and 17p allelic loss in medulloblastoma. Cancer Res., **62**, 3794–3797.
19. Costello,J., Fruhwald,M., Smiraglia,D., Rush,L., Robertson,G., Gao,X., Wright,F., Feramisco,J., Peltomaki,P., Lang,J. *et al.* (2000) Aberrant CpG-island methylation has non-random and tumour-type-specific patterns. *Nat. Genet.*, **24**, 132–138.
20. Schatz,P., Dietrich,D. and Schuster,M. (2004) Rapid analysis of CpG methylation patterns using RNase T1 cleavage and MALDI-TOF. *Nucleic Acids Res.*, **32**, e167.
21. Ching,T-T., Maunakea,A.K., Jun,P., Hong,C., Zardo,G., Pinkel,D., Albertson,D.G., Fridlyand,J., Mao,J.-H., Shchors,K. *et al.* (2005) Epigenome analyses using BAC microarrays identify evolutionary conservation of tissue-specific methylation of SHANK3. *Nat. Genet.*, **37**, 645–651.
22. Hatada,I., Fukasawa,M., Kimura,M., Morita,S., Yamada,K., Yoshikawa,T., Yamanaka,S., Endo,C., Sakurada,A., Sato,M. *et al.* (2006) Genome-wide profiling of promoter methylation in human. *Oncogene*, **25**, 3059–3064.
23. Huang,T., Perry,M. and Laux,D. (1999) Methylation profiling of CpG islands in human breast cancer cells. *Hum. Mol. Genet.*, **8**, 459–470.
24. van Doorn,R., Zoutman,W.H., Dijkman,R., de Menezes,R.X., Commandeur,S., Mulder,A.A., van der Velden,P.A., Vermeer,M.H., Willemze,R., Yan,P.S. *et al.* (2005) Epigenetic profiling of cutaneous T-cell lymphoma: promoter hypermethylation of multiple tumor suppressor genes including BCL7a, PTPRG, and p73. *J. Clin. Oncol.*, **23**, 3886–3896.
25. Yan,P.S., Perry,M.R., Laux,D.E., Asare,A.L., Caldwell,C.W. and Huang,TH-M. (2000) CpG island arrays: an application toward deciphering epigenetic signatures of breast cancer. *Clin. Cancer Res.*, **6**, 1432–1438.
26. Adrien,L., Schlecht,N., Kawachi,N., Smith,R., Brandwein-Gensler,M., Massimi,A., Chen,S., Prystowsky,M., Childs,G. and Belbin,T. (2006) Classification of DNA methylation patterns in tumor cell genomes using a CpG island microarray. *Cytogenet. Genome. Res.*, **114**, 16–23.
27. Weber,M., Davies,J.J., Wittig,D., Oakeley,E.J., Haase,M., Lam,W.L. and Schubeler,D. (2005) Chromosome-wide and promoter-specific analyses identify sites of differential DNA methylation in normal and transformed human cells. *Nat. Genet.*, **37**, 853–862.
28. Rauch,T., Li,H., Wu,X. and Pfeifer,G.P. (2006) MIRA-assisted microarray analysis, a new technology for the determination of DNA methylation patterns, identifies frequent methylation of homeodomain-containing genes in lung cancer cells. *Cancer Res.*, **66**, 7939–7947.
29. Lee,D.U., Agarwal,S. and Rao,A. (2002) Th2 lineage commitment and efficient IL-4 production involves extended demethylation of the IL-4 gene. *Immunity*, **16**, 649–660.
30. Palmer,L., Rabinowicz,P., O'Shaughnessy,A., Balija,V., Nascimento,L., Dike,S., de la Bastide,M., Martienssen,R. and McCombie,W. (2003) Maize genome sequencing by methylation filtration. *Science*, **302**, 2115–2117.
31. Rollins,R.A., Haghighi,F., Edwards,J.R. Das, R., Zhang, M.Q., Ju, J. and Bestor, T.H. (2006) Large-scale structure of genomic methylation patterns. *Genome. Res.*, **16**, 157–163.

32. Nouzova,M., Holtan,N., Oshiro,M., Isett,R., Munoz-Rodriguez,J., List,A., Narro,M., Miller,S., Merchant,N. and Futscher,B. (2004) Epigenomic changes during leukemia cell differentiation: analysis of histone acetylation and cytosine methylation using CpG island microarrays. *J. Pharmacol. Exp. Ther.*, **311**, 968–981.
33. Cross,S., Charlton,J., Nan,X. and Bird,A. (1994) Purification of CpG islands using a methylated DNA binding column. *Nat. Genet.*, **6**, 236–244.
34. Groot,G. and Kroon,A. (1979) Mitochondrial DNA from various organisms does not contain internally methylated cytosine in -CCGG-sequences. *Biochim. Biophys. Acta*, **564**, 355–357.
35. Ibrahim,A.E.K., Thorne,N.P., Baird,K., Barbosa-Morais, N.L., Tavare, S., Collins, V.P., Wyllie, A.H., Arends, M.J. and Brenton, J.D. (2006) MMASS: an optimized array-based method for assessing CpG island methylation. Nucleic Acids Res., **34**, e136.
36. Fraga,M.F., Ballestar,E., Paz,M.F., Ropero,S., Setien,F., Ballestar,M.L., Heine-Suner,D., Cigudosa,J.C., Urioste,M., Benitez,J. *et al.* (2005) From The Cover: Epigenetic differences arise during the lifetime of monozygotic twins. *Proc. Natl. Acad. Sci. USA*, **02**, 10604–10609.
37. Toyota,M., Ahuja,N., Ohe-Toyota,M., Herman,J.G., Baylin,S.B. and Issa,J-P.J. (1999) CpG island methylator phenotype in colorectal cancer. *Proc. Natl. Acad. Sci. USA*, **96**, 8681–8686.
38. Grinberg,I. and Millen,K.J. (2005) The ZIC gene family in development and disease. *Clin. Genet.*, **67**, 290–296.
39. Brown,L.Y., Odent,S., David,V., Blayau,M., Dubourg,C., Apacik,C., Delgado,M.A., Hall,B.D., Reynolds,J.F., Sommer,A. *et al.* (2001) Holoprosencephaly due to mutations in ZIC2: alanine tract expansion mutations may be caused by parental somatic recombination. *Hum. Mol. Genet.*, **10**, 791–796.
40. Pomeroy,S.L., Tamayo,P., Gaasenbeek,M., Sturla,L.M., Angelo,M, McLaughlin,M.E., Kim,J.Y.H., Goumnerova,L.C., Black,P.M., Lau,C. *et al.* (2002) Prediction of central nervous system embryonal tumour outcome based on gene expression. *Nature*, **415**, 436–442.
41. Sakurada,T., Mima,K., Kurisaki,A., Sugino,H. and Yamauchi,T. (2005) Neuronal cell type-specific promoter of the [alpha] CaM kinase II gene is activated by Zic2, a Zic family zinc finger protein. *Neurosci. Res.*, **53**, 323–330.
42. Liu,H. and Grundstrom,T. (2002) Calcium regulation of GM-CSF by calmodulin-dependent kinase II phosphorylation of Ets1. *Mol. Biol. Cell*, **13**, 4497–4507.
43. Ishitani,T., Kishida,S., Hyodo-Miura,J. *et al.* (2003) The TAK1-NLK mitogen-activated protein kinase cascade functions in the Wnt-5a/Ca^{2+} pathway to antagonize Wnt/{beta}-catenin signaling. *Mol. Cell. Biol.*, **23**, 131–139.
44. Koyabu,Y., Nakata,K., Mizugishi,K., Aruga,J. and Mikoshiba,K. (2001) Physical and functional interactions between Zic and Gli proteins. *J. Biol. Chem.*, **276**, 6889–6892.
45. Mendrzyk,F., Radlwimmer,B., Joos,S., Kokocinski,F., Benner,A., Stange,D.E., Neben,K., Fiegler,H., Carter,N.P., Reifenberger,G. *et al.* (2005) Genomic and protein expression profiling identifies CDK6 as novel independent prognostic marker in medulloblastoma. *J. Clin. Oncol.*, **23**, 8853–8862.
46. Van den Boom,J., Wolter,M., Kuick,R. *et al.* (2003) Characterization of gene expression profiles associated with glioma progression using oligonucleotide-based microarray analysis and real-time reverse transcription-polymerase chain reaction. *Am. J. Pathol.*, **163**, 1033–1043.
47. Klein,C., Schmidt-Kittler,O., Schardt,J., Pantel,K., Speicher,M. and Riethmuller,G. (1999) Comparative genomic hybridization, loss of heterozygosity, and DNA sequence analysis of single cells. *Proc. Natl. Acad. Sci. USA*, **96**, 4494–4499.
48. Zielinski,B., Gratias,S., Toedt,G. *et al.* (2005) Detection of chromosomal imbalances in retinoblastoma by matrix-based comparative genomic hybridization. *Genes Chromosomes Cancer*, **43**, 294–301.
49. Smyth,G., Yang,Y. and Speed,T. (2003) Statistical issues in cDNA microarray data analysis. *Methods Mol. Biol.*, **224**, 111–136.
50. Yang,Y. and Thorne,N. (2003) Normalization for two-color cDNA microarray data. Science and Statistics: A Festschrift for Terry Speed, IMS Lecture Notes, Monograph Series, 40, 403–418. Goldstein DR, series editor.
51. Pfaffl,M.W. (2001) A new mathematical model for relative quantification in real-time RT-PCR. *Nucleic Acids Res.*, **29**, e45.
52. Gardiner-Garden,M. and Frommer,M. (1987) CpG Islands in vertebrate genomes. *J. Mol. Biol.*, **196**, 261–282.